JACS
JOURNAL OF THE AMERICAN CHEMICAL SOCIETY

Communication

pubs.acs.org/JACS

Hierarchical Self-Assembly of Responsive Organoplatinum(II) Metallacycle–TMV Complexes with Turn-On Fluorescence

Ye Tian,[†,#] Xuzhou Yan,[‡,#] Manik Lal Saha,[‡] Zhongwei Niu,[*,†] and Peter J. Stang[*,‡]

[†]Key Laboratory of Photochemical Conversion and Optoelectronic Materials, Technical Institute of Physics and Chemistry, Chinese Academy of Sciences, Beijing 100190, China

[‡]Department of Chemistry, University of Utah, 315 South 1400 East, Room 2020, Salt Lake City, Utah 84112, United States

Supporting Information

ABSTRACT: Here we report that the rod-like tobacco mosaic virus (TMV), having a negatively charged surface, can be assembled into three-dimensional micrometer-sized bundle-like superstructures via multiple electrostatic interactions with a positively charged molecular "glue", namely, a tetraphenylethylene (TPE)-based discrete organoplatinum(II) metallacycle (**TPE-Pt-MC**). Due to the nanoconfinement effect in the resultant **TMV/TPE-Pt-MC** complexes and the aggregation-induced emission (AIE) activity of the TPE units, these hierarchical architectures result in a dramatic fluorescence enhancement that not only provides evidence for the formation of novel metal–organic biohybrid materials but also represents an alternative to turn-on fluorescence. Moreover, the dissociation of these final constructs and subsequent release of individual virus have been achieved by disrupting the **TPE-Pt-MC** core using tetrabutylammonium bromide (TBAB). This strategy is also compatible with other protein-based nanoparticles such as bacteriophage M13 and ferritin, proving the generality of this approach. Hence, this research will open new routes for the fabrication of functional biohybrid materials involving metal–organic complexes and anisotropically shaped bionanoparticles.

Well-defined hierarchical architectures based on anisotropic nanoparticles exist extensively in nature, from the centrioles in animal cells[1] to the Clio pyramidata shell[2] and the chameleon derma.[3] Benefiting from their special optical, electronic, and mechanical properties, these anisotropic particles are becoming candidates in constructing artificial systems, such as artificial neural networks,[4] semiconductor nanorod-based superparticles,[5] and Au nanorod helical superstructures.[6] The one-dimensional (1D) rod-like tobacco mosaic virus (TMV) with its complex physicochemical properties yet monodispersed and anisotropic morphology offers an ideal building block for hierarchical assemblies. TMV measures 300 nm in length and 18 nm in diameter with a 4.0 nm cavity, and 2130 coat proteins helically around its RNA.[7] The isoelectric point (pI) of TMV is ~3.5, so it is negatively charged under neutral conditions. In recent years, through the self-assembly of TMV, scientists have developed many novel materials, such as water-soluble conductive nanowires,[8] oriented surfaces for directing cell growth,[9] and thermoresponsive superlattices with tunable distances.[10] However, how to evaluate the hierarchical assembly via a direct observation and realize the reversible disassembly into the individual virus still represents a big challenge.

Coordination-driven self-assembly is a well-established methodology to elegantly construct supramolecular coordination complexes (SCCs) with well-defined shapes and sizes by the spontaneous formation of dative metal–ligand bonds.[11] Some inherent features of SCCs, such as easy tunability of the dimensions of a metallacycle or metallacage with minimal synthetic redesign, the versatility of the metal and ligand precursors, facile incorporation of functional groups through pre- or postassembly modification, and rich host–guest chemistry associated with the internal cavities, make them widely applicable in materials science and biotechnology.[12] Recently, quite a few light-emitting metal–organic materials on SCC platforms are reported and their structure–property relationships have been investigated to tune and achieve the desired photophysics.[13] Aggregation-induced emission (AIE), first reported by Tang,[14] describes the phenomenon that fluorogens exhibit almost no fluorescence as discrete molecules but become highly emissive in the condensed state. We utilized AIE-active ligands to construct a library of highly emissive organoplatinum(II) metallacycles and metallacages and explored the influences of structural factors on their optical properties.[13c,d] Having established the chemistry of highly emissive SCCs, we are now pursuing the goal of preparing their functional biohybrid materials by hierarchical self-assembly with viruses, then tracing the assembly processes via fluorescence signals and studying their 3D nanoscale morphologies.

Electrostatic interaction involves the attraction of ions or molecules with fully opposite charges, which is not only crucial in determining and maintaining the 3D structures and functions of large biomolecules,[15] but also heavily influences the fabrication and construction of controllable supramolecular materials, especially involving tunable nanoscale assemblies[16] and healable soft matter with high strength and viscoelasticity.[17] To achieve a TMV-based hierarchical self-assembly and to realize the visualization of the assembly process, we chose an organo-Pt(II) metallacycle that has multiple positive charges and possesses AIE features, as a molecular "glue". This design will solve the aforesaid issues because: (i) it can intrinsically aid the resultant hierarchical self-assembly with turn-on AIE-based fluorescence, which can also be used as a handle to probe the assembly processes, and (ii) the dynamic nature of the metallocyclic core endows the

Received: July 18, 2016
Published: September 8, 2016

ACS Publications © 2016 American Chemical Society

DOI: 10.1021/jacs.6b07402
J. Am. Chem. Soc. 2016, 138, 12033–12036

biohybrid materials with reversibility, providing a means of realizing the subsequent release of the individual virus. These unique features are hardly achievable by other cationic species.

Herein, we present the design and construction of a light-emitting 3D biohybrid complex by hierarchical self-assembly of 1D rod-like TMV and 2D discrete organoplatinum(II) metallacycle via electrostatic interactions (Scheme 1). Specifically, a

Scheme 1. Cartoon Representation of the Formation of a Light-Emitting Metal−Organic Biohybrid Complex via Hierarchical Self-Assembly of a Discrete Organoplatinum(II) Metallacycle and Tobacco Mosaic Virus

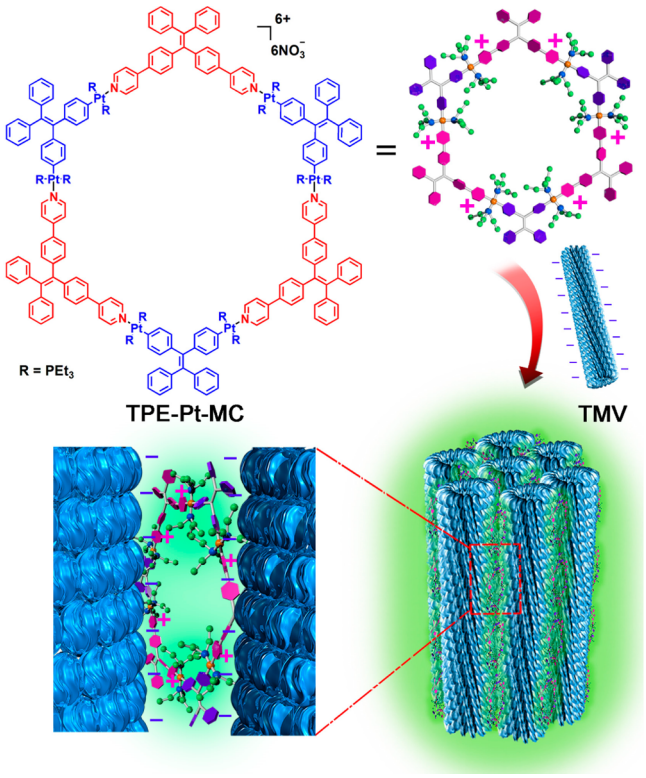

TPE-based discrete organoplatinum(II) metallacycle (**TPE-Pt-MC**) with ca. 4.0 × 6.0 nm cavity and six positive charges[13d] was employed to induce the hierarchical self-assembly of negatively charged TMV to form 3D biohybrid complexes. Photophysical studies showed marked fluorescence enhancement upon the addition of TMV into the **TPE-Pt-MC** solution due to the nanoconfinement effect associated with the biohybrid complex formation. This represents a novel approach for turn-on fluorescence in addition to AIE. Furthermore, disassembly of the complex is attributed to the disruption of the **TPE-Pt-MC** by TBAB, and the subsequent release of the rod-like virus. As such, this work exploits the charges, functionality, reversibility, and skeleton of **TPE-Pt-MC** to realize the reversible construction of hierarchically ordered metal−organic biohybrid complex.

The formation of the **TMV/TPE-Pt-MC** biohybrid complex was accomplished by simply mixing the TMV/H_2O solution with a **TPE-Pt-MC**/DMSO solution. Transmission electron microscopy (TEM) was used to visualize the formation of the aggregates from TMV and **TPE-Pt-MC** via electrostatic interactions. The TEM image of the native TMV exhibited a discrete 1D rod-like shape with a monodispersed diameter of ca. 18 nm (Figure S1). Following the addition of **TPE-Pt-MC**, larger aggregates, showing network-like morphology with several micrometers, were observed (Figure 1a). The networks were composed of bundle-like structures measuring a dozen to

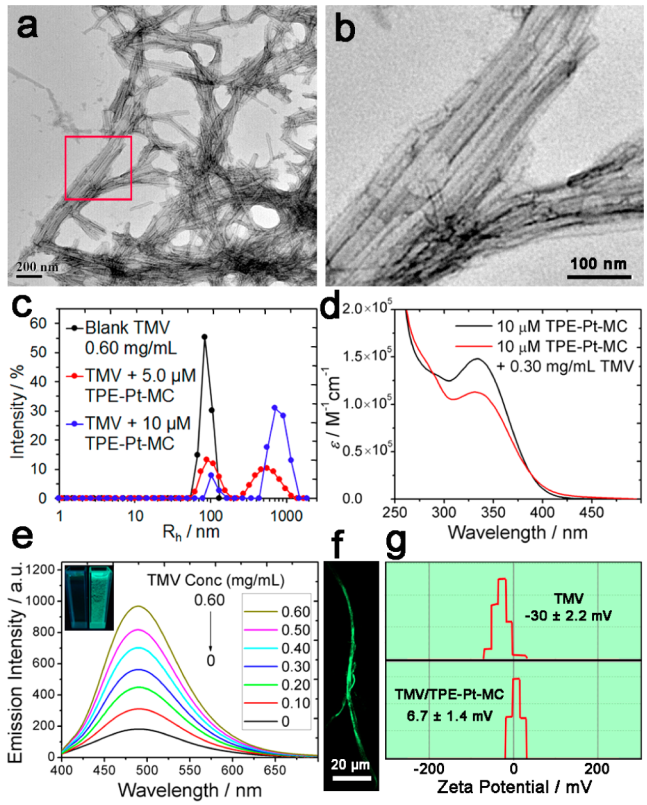

Figure 1. (a,b) TEM images of **TMV/TPE-Pt-MC** complexes, by negative staining with 2.0% (*w*/*v*) uranyl acetate aqueous solution. (c) DLS profiles of 0.60 mg/mL TMV self-assembly with 0, 5.0, and 10 μM TPE-Pt-MC. (d) Absorption spectra of the **TPE-Pt-MC** and **TMV/TPE-Pt-MC** complex. (e) Emission spectra of 10 μM **TPE-Pt-MC** with the addition of different concentrations of TMV. Inset: Photographs of 10 μM **TPE-Pt-MC** with the addition of 0 (left) and 0.60 (right) mg/mL of TMV upon UV lamp excitation (λ_{ex} = 365 nm). (f) The confocal laser scanning microscopy (CLSM) image for the **TMV/TPE-Pt-MC** biohybrid complexes. (g) Zeta potential of native TMV and **TMV/TPE-Pt-MC** complex at a TMV concentration of 0.6 mg/mL and a **TPE-Pt-MC** concentration of 10 μM.

hundreds of nanometers. A magnified image revealed that the TMV aligned with each other tightly in the complexes, showing well-ordered arrays (Figure 1b). In addition, the individual TMV in the biohybrid complex showed the same diameter (ca. 18 nm) as the native one. Dynamic light scattering (DLS) provided further support for the formation of **TMV/TPE-Pt-MC** biohybrid complexes (Figure 1c). The hydrodynamic radius (R_h) of TMV (0.60 mg/mL) in a solution of H_2O/DMSO (3/7, *v*/*v*) was 109 nm. Addition of **TPE-Pt-MC** induced the formation of larger aggregates and, simultaneously, the gradual disappearance of free TMV. The size of the **TMV/TPE-Pt-MC** complexes increased with the addition of the **TPE-Pt-MC** to ~635 nm at a **TPE-Pt-MC** concentration of 5.0 μM and to ~814 nm upon increasing the concentration of **TPE-Pt-MC** to 10 μM. By analyzing the scattering intensity, it was established that the percentage of the free TMV peak decreased from 100% to only 10%.

We previously reported that the **TPE-Pt-MC** exhibited a sharp absorption band at around 340 nm in CH_2Cl_2, and this band underwent minor shifts with different molar absorption

DOI: 10.1021/jacs.6b07402
J. Am. Chem. Soc. 2016, 138, 12033−12036

coefficients (ε) upon counteranion changes.[13d] In a solution of H_2O/DMSO (3/7, v/v), the free **TPE-Pt-MC** exhibited a similar absorption band at 334 nm with ε of 1.48×10^5 M^{-1} cm^{-1} (Figure 1d). Upon the addition of TMV, this band slightly shifted to 331 nm with a decreased ε of 1.28×10^5 M^{-1} cm^{-1}, providing evidence for the electrostatic interactions between the positively charged **TPE-Pt-MC** and the negatively charged TMV.

To investigate the aggregation effect of **TPE-Pt-MC** associated with the coassembly, fluorescence emission profiles of the **TMV/TPE-Pt-MC** complexes were recorded (Figure 1e). In the absence of TMV, the **TPE-Pt-MC** is weakly emissive at ca. 490 nm in H_2O/DMSO (3/7, v/v). Through the addition of TMV, the twisted TPE moieties became rigidified in the confined environment provided by the tight and well-ordered TMV arrays (Scheme 1 and Figure 1b), thus causing a marked fluorescence enhancement. From a time scan spectrum (Figure S2) it was further observed that the emission intensity at 490 nm enhanced gradually and then reached an equilibrium after 120 s, suggesting that the assembly process is sufficiently fast. Likewise, the emission intensity of the **TPE-Pt-MC** increased with the addition of TMV, showing a linear relationship in the concentration range of 0−0.60 mg/mL (Figure S3). The **TMV/TPE-Pt-MC** biohybrid complexes exhibited a 5.41-fold fluorescence enhancement over free **TPE-Pt-MC** at a TMV concentration of 0.60 mg/mL and a **TPE-Pt-MC** concentration of 10 μM. There was no shift of the maximum emission band (490 nm), indicating that the fluorescence enhancement is due to the aggregation of the TPE moieties.[18] With a UV lamp, one can distinguish by the naked eye that the nonemissive **TPE-Pt-MC** solution is strongly emissive in the presence of TMV. Furthermore, the confocal laser scanning microscopy (CLSM) image clearly shows the **TMV/TPE-Pt-MC** biohybrid complexes with a strong green emission (Figure 1f), further suggesting that the AIE property of the **TPE-Pt-MC** was activated by the nanoconfinement effect in the **TMV/TPE-Pt-MC** biohybrid complexes.

The zeta potential (ξ) was also measured to investigate the mechanism for this assembly. As shown in Figure 1g, native TMV has $\xi = -30 \pm 2.2$ mV in H_2O/DMSO (3/7, v/v). By coassembling with **TPE-Pt-MC**, the surface charge of the **TMV/TPE-Pt-MC** complex is nearly neutral, indicating that the coassembly of TMV and **TPE-Pt-MC** is driven via electrostatic interactions.

For such 3D hierarchical architectures based on bionanoparticles, reversible disassembly is a critical process for their applications in the delivery and release of compounds.[19] It was previously reported that TBAB can disrupt the metal−ligand bonds, thus damaging both the metallacyclic core and the positive charges of the **TPE-Pt-MC**.[12d] Hence, we investigated the disassembly of the **TMV/TPE-Pt-MC** complexes by treating them with TBAB. In the TEM image (Figure 2a), the individual virus with a diameter of ca. 18 nm was observed again, indicating the breakup of the **TMV/TPE-Pt-MC** biohybrid complexes and the release of viruses. DLS experiments revealed that addition of 50.0 μM TBAB into the **TMV/TPE-Pt-MC** complexes allowed partial dissociation, and the R_h of the complexes decreased from ~814 to ~150 nm (Figure 2b). Upon increasing the TBAB concentration to 100 μM, most of the viruses were free and the peak corresponding to free TMV at ~63 nm was observed (Figure 2b). This decreased R_h and virus length (<300 nm) compared with the native TMV indicated that the TMV was slightly broken during the assembly and disassembly processes, which oftentimes happens during the bioconjugation of TMV.[20]

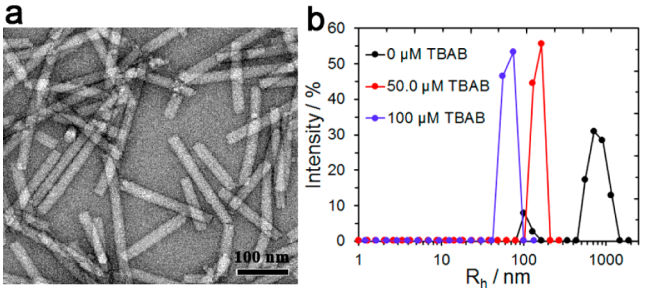

Figure 2. (a) TEM image of the released individual TMV nanoparticles by the addition of 100 μM TBAB. (b) DLS profiles of **TMV/TPE-Pt-MC** complexes with the addition of 0, 50.0, and 100 μM TBAB.

Since most viruses are negatively charged, we hypothesized that this is a general method for preparing functional biohybrid materials involving metal−organic complexes and anisotropically shaped bionanoparticles. To test this, we investigated the assembly of bacteriophage M13, which is a filamentous virus with a 6.6 nm diameter and a 880 nm length (Figure S4). Native M13 has a pI value of ~4.3. The TEM image shown in Figure 3a

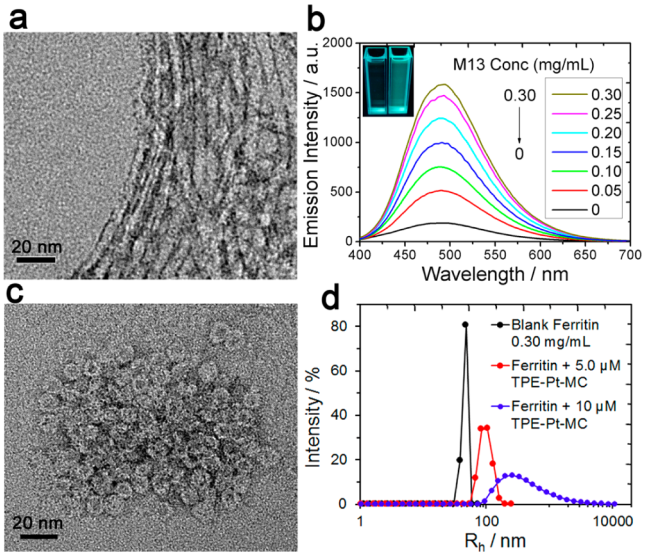

Figure 3. (a) TEM image of **M13/TPE-Pt-MC** complexes, by negative staining with 2.0% (w/v) uranyl acetate aqueous solution. (b) Emission spectra of 10 μM **TPE-Pt-MC** with the addition of M13. Inset: Photographs of 10 μM **TPE-Pt-MC** with the addition of 0 (left) and 0.30 (right) mg/mL of M13 upon UV lamp excitation (λ_{ex} = 365 nm). (c) TEM image of **ferritin/TPE-Pt-MC** complexes, by negative staining with 2.0% (w/v) uranyl acetate aqueous solution. (d) DLS profiles of 0.30 mg/mL of ferritin upon self-assembly with 0, 5.0, and 10 μM of **TPE-Pt-MC**.

demonstrated that M13 also formed **M13/TPE-Pt-MC** complexes due to electrostatic interactions. In the fluorescence emission profiles, M13 has a similar fluorescence enhancement effect on **TPE-Pt-MC** as TMV (Figure 3b). Due to the smaller diameter and thus the larger surface area, M13 has a higher fluorescence enhancement capacity than TMV under the same conditions. At a M13 concentration of 0.3 mg/mL, the emission intensity of the **M13/TPE-Pt-MC** complexes at 490 nm showed a 9.58-fold enhancement over that of the free **TPE-Pt-MC** at 10 μM. However, because of the high aspect ratio and flexible feature, DLS is not suitable for characterizing the size of the M13 and **M13/TPE-Pt-MC** complexes.

DOI: 10.1021/jacs.6b07402
J. Am. Chem. Soc. 2016, 138, 12033−12036

Ferritin is a globular protein complex measuring 12 nm in diameter (Figure S5) and has a pI value of ~4.5. **Ferritin/TPE-Pt-MC** complexes were also clearly formed by the addition of **TPE-Pt-MC** as shown by the TEM images (Figure 3c). In contrast to TMV and M13, ferritin has broad absorbance spanning 250−500 nm (Figure S6) that entirely covers the sharp absorption band of **TPE-Pt-MC** at 334 nm in the **ferritin/TPE-Pt-MC** complexes (Figure S7). At the same time, ferritin shows a weak fluorescence enhancement effect (Figure S8) as well as a blue shift from 490 to 481 nm in the emission spectrum of **ferritin/TPE-Pt-MC** complexes. This is likely due to the globular morphology of ferritin. Upon the increase of the **TPE-Pt-MC** concentrations, the **ferritin/TPE-Pt-MC** complexes undergo further aggregation, as expected. The aggregate size increased from ~46 nm (native ferritins) to ~99 nm (0.5 μM **TPE-Pt-MC** added) and to ~560 nm (10 μM **TPE-Pt-MC** added) (Figure 3d). These results demonstrate that this is a general method to form bionanoparticle/**TPE-Pt-MC** hybrid complexes.

In summary, we have described the first case of the hierarchical self-assembly of a rod-like TMV virus with a TPE-based discrete organoplatinum(II) metallacycle through electrostatic interactions, in which the TMV aligned with each other in well-ordered arrays. Due to the nanoconfinement effect in the resultant architectures, the AIE property of the **TPE-Pt-MC** results in markedly enhanced fluorescence. In addition, the dissociation of the **TMV/TPE-Pt-MC** complexes and subsequent release of individual virus nanoparticles are achieved by disrupting the core of the **TPE-Pt-MC** using TBAB. Furthermore, in view of the fact that most viruses have a pI value of 3.5−5.5, this method is general and also works for other protein-based species, like bacteriophage M13 and ferritin, which formed emissive bionanoparticle/**TPE-Pt-MC** hybrid complexes. Such hierarchical architectures with AIE activity and disassembly capacity are attractive candidates for dynamic optical materials or as biocarriers.

■ ASSOCIATED CONTENT

Supporting Information

The Supporting Information is available free of charge on the ACS Publications website at DOI: 10.1021/jacs.6b07402.

Experimental details and additional data (PDF)

■ AUTHOR INFORMATION

Corresponding Authors

*niu@mail.ipc.ac.cn

*stang@chem.utah.edu

Author Contributions

#These authors contributed equally to this work.

Notes

The authors declare no competing financial interest.

■ ACKNOWLEDGMENTS

This work was supported by the 973 Program (2013CB933800) and National Natural Science Foundation of China (Grant No. 51303191, 21304103, 21474123, and 51173198). P.J.S. thanks the NSF (Grant 1212799) for financial support.

■ REFERENCES

(1) Hilbert, M.; Noga, A.; Frey, D.; Hamel, V.; Guichard, P.; Kraatz, S. H. W.; Pfreundschuh, M.; Hosner, S.; Fluckiger, I.; Jaussi, R.; Wieser, M. M.; Thieltges, K. M.; Deupi, X.; Muller, D. J.; Kammerer, R. A.; Gonczy, P.; Hirono, M.; Steinmetz, M. O. *Nat. Cell Biol.* **2016**, *18*, 393.

(2) Li, L.; Weaver, J. C.; Ortiz, C. *Nat. Commun.* **2015**, *6*, 6216.

(3) Teyssier, J.; Saenko, S. V.; van der Marel, D.; Milinkovitch, M. C. *Nat. Commun.* **2015**, *6*, 6368.

(4) Escarcega-Bobadilla, M. V.; Zelada-Guillen, G. A.; Pyrlin, S. V.; Wegrzyn, M.; Ramos, M. M.; Gimenez, E.; Stewart, A.; Maier, G.; Kleij, A. W. *Nat. Commun.* **2013**, *4*, 2648.

(5) Wang, T.; Zhuang, J.; Lynch, J.; Chen, O.; Wang, Z.; Wang, X.; LaMontagne, D.; Wu, H.; Wang, Z.; Cao, Y. C. *Science* **2012**, *338*, 358.

(6) Lan, X.; Lu, X.; Shen, C.; Ke, Y.; Ni, W.; Wang, Q. *J. Am. Chem. Soc.* **2015**, *137*, 457.

(7) (a) Liu, Z.; Qiao, J.; Niu, Z.; Wang, Q. *Chem. Soc. Rev.* **2012**, *41*, 6178. (b) Liu, Z.; Niu, Z. *Chin. J. Polym. Sci.* **2014**, *32*, 1271.

(8) Niu, Z.; Liu, J.; Lee, L. A.; Bruckman, M. A.; Zhao, D.; Koley, G.; Wang, Q. *Nano Lett.* **2007**, *7*, 3729.

(9) Lin, Y.; Balizan, E.; Lee, L. A.; Niu, Z.; Wang, Q. *Angew. Chem., Int. Ed.* **2010**, *49*, 868.

(10) Li, T.; Zan, X.; Winans, R. E.; Wang, Q.; Lee, B. *Angew. Chem., Int. Ed.* **2013**, *52*, 6638.

(11) (a) Chakrabarty, R.; Mukherjee, P. S.; Stang, P. J. *Chem. Rev.* **2011**, *111*, 6810. (b) Cook, T. R.; Stang, P. J. *Chem. Rev.* **2015**, *115*, 7001. (c) Lifchitz, A. M.; Rosen, M. S.; McGuirk, C. M.; Mirkin, C. A. *J. Am. Chem. Soc.* **2015**, *137*, 7252. (d) Newkome, G. R.; Moorefield, C. N. *Chem. Soc. Rev.* **2015**, *44*, 3954.

(12) (a) Inokuma, Y.; Kawano, M.; Fujita, M. *Nat. Chem.* **2011**, *3*, 349. (b) Yan, X.; Li, S.; Pollock, J. B.; Cook, T. R.; Chen, J.; Zhang, Y.; Ji, X.; Yu, Y.; Huang, F.; Stang, P. J. *Proc. Natl. Acad. Sci. U. S. A.* **2013**, *110*, 15585. (c) Cook, T. R.; Vajpayee, V.; Lee, M. H.; Stang, P. J.; Chi, K.-W. *Acc. Chem. Res.* **2013**, *46*, 2464. (d) Li, Z.-Y.; Zhang, Y.; Zhang, C.-W.; Chen, L.-J.; Wang, C.; Tan, H.; Yu, Y.; Li, X.; Yang, H.-B. *J. Am. Chem. Soc.* **2014**, *136*, 8577. (e) Wang, M.; Wang, C.; Hao, X.-Q.; Li, X.; Vaughn, T. J.; Zhang, Y.-Y.; Yu, Y.; Li, Z.-Y.; Song, M.-P.; Yang, H.-B.; Li, X. *J. Am. Chem. Soc.* **2014**, *136*, 10499. (f) Foster, J. A.; Parker, R. M.; Belenguer, A. M.; Kishi, N.; Sutton, S.; Abell, C.; Nitschke, J. R. *J. Am. Chem. Soc.* **2015**, *137*, 9722. (g) Brown, C. J.; Toste, F. D.; Bergman, R. G.; Raymond, K. N. *Chem. Rev.* **2015**, *115*, 3012. (h) Bhat, I. A.; Samanta, D.; Mukherjee, P. S. *J. Am. Chem. Soc.* **2015**, *137*, 9497. (i) Zhou, Z.; Yan, X.; Cook, T. R.; Saha, M. L.; Stang, P. J. *J. Am. Chem. Soc.* **2016**, *138*, 806.

(13) (a) Roy, B.; Ghosh, A. K.; Srivastava, S.; D'Silva, P.; Mukherjee, P. S. *J. Am. Chem. Soc.* **2015**, *137*, 11916. (b) Yamashina, M.; Sartin, M. M.; Sei, Y.; Akita, M.; Takeuchi, S.; Tahara, T.; Yoshizawa, M. *J. Am. Chem. Soc.* **2015**, *137*, 9266. (c) Yan, X.; Cook, T. R.; Wang, P.; Huang, F.; Stang, P. J. *Nat. Chem.* **2015**, *7*, 342. (d) Yan, X.; Wang, M.; Cook, T. R.; Zhang, M.; Saha, M. L.; Zhou, Z.; Li, X.; Huang, F.; Stang, P. J. *J. Am. Chem. Soc.* **2016**, *138*, 4580.

(14) Luo, J.; Xie, Z.; Lam, J. W. Y.; Cheng, L.; Chen, H.; Qiu, C.; Kwok, H. S.; Zhan, X.; Liu, Y.; Zhu, D.; Tang, B. Z. *Chem. Commun.* **2001**, 1740.

(15) Okazaki, K.; Sato, T.; Takano, M. *J. Am. Chem. Soc.* **2012**, *134*, 8918.

(16) (a) Düring, J.; Hölzer, A.; Kolb, U.; Branscheid, R.; Gröhn, F. *Angew. Chem., Int. Ed.* **2013**, *52*, 8742. (b) Suzuki, Y.; Cardone, G.; Restrepo, D.; Zavattieri, P. D.; Baker, T. S.; Tezcan, F. A. *Nature* **2016**, *533*, 369. (c) Song, W. J.; Tezcan, F. A. *Science* **2014**, *346*, 1525.

(17) Sun, T. L.; Kurokawa, T.; Kuroda, S.; Ihsan, A. B.; Akasaki, T.; Sato, K.; Haque, M. A.; Nakajima, T.; Gong, J. P. *Nat. Mater.* **2013**, *12*, 932.

(18) Chen, L.-J.; Ren, Y. Y.; Wu, N. W.; Sun, B.; Ma, J. Q.; Zhang, L.; Tan, H.; Liu, M.; Li, X.; Yang, H.-B. *J. Am. Chem. Soc.* **2015**, *137*, 11725.

(19) Kostiainen, M. A.; Kasyutich, O.; Cornelissen, J. J. L. M.; Nolte, R. J. M. *Nat. Chem.* **2010**, *2*, 394.

(20) Tian, Y.; Gao, S.; Wu, M.; Liu, X.; Qiao, J.; Zhou, Q.; Jiang, S.; Niu, Z. *ACS Appl. Mater. Interfaces* **2016**, *8*, 10800.

DOI: 10.1021/jacs.6b07402
J. Am. Chem. Soc. 2016, 138, 12033−12036